NEURAL REGENERATION RESEARCH
www.nrronline.org

Research Article

Ferroptosis inhibition protects vascular endothelial cells and maintains integrity of the blood-spinal cord barrier after spinal cord injury

Wenxiang Li[1, #], Xiaoqing Zhao[1, #], Rong Zhang[1, #], Xinjie Liu[2], Zhangyang Qi[1], Yang Zhang[1], Weiqi Yang[1], Yilin Pang[2], Chenxi Zhao[1], Baoyou Fan[2], Ning Ran[1], Jiawei Zhang[2], Xiaohong Kong[1], Shiqing Feng[1, 2, *], Xue Yao[1, 2, *]

https://doi.org/10.4103/1673-5374.371377
Date of submission: August 3, 2022
Date of decision: November 8, 2022
Date of acceptance: December 21, 2022
Date of web publication: March 15, 2023

From the Contents

Graphical Abstract

Inhibition of endothelial cell ferroptosis maintains blood-spinal cord barrier integrity to promote spinal cord injury recovery

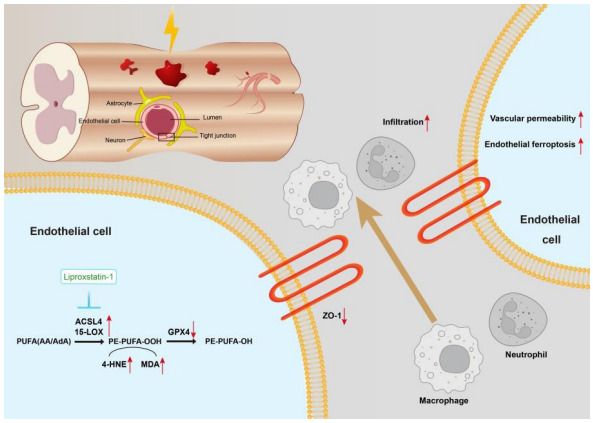

Abstract

Maintaining the integrity of the blood-spinal cord barrier is critical for the recovery of spinal cord injury. Ferroptosis contributes to the pathogenesis of spinal cord injury. We hypothesized that ferroptosis is involved in disruption of the blood-spinal cord barrier. In this study, we administered the ferroptosis inhibitor liproxstatin-1 intraperitoneally after contusive spinal cord injury in rats. Liproxstatin-1 improved locomotor recovery and somatosensory evoked potential electrophysiological performance after spinal cord injury. Liproxstatin-1 maintained blood-spinal cord barrier integrity by upregulation of the expression of tight junction protein. Liproxstatin-1 inhibited ferroptosis of endothelial cell after spinal cord injury, as shown by the immunofluorescence of an endothelial cell marker (rat endothelium cell antigen-1, RECA-1) and ferroptosis markers Acyl-CoA synthetase long-chain family member 4 and 15-lipoxygenase. Liproxstatin-1 reduced brain endothelial cell ferroptosis *in vitro* by upregulating glutathione peroxidase 4 and downregulating Acyl-CoA synthetase long-chain family member 4 and 15-lipoxygenase. Furthermore, inflammatory cell recruitment and astrogliosis were mitigated after liproxstatin-1 treatment. In summary, liproxstatin-1 improved spinal cord injury recovery by inhibiting ferroptosis in endothelial cells and maintaining blood-spinal cord barrier integrity.
Key Words: blood-spinal cord barrier; ferroptosis; liproxstatin-1; neuroinflammation; spinal cord injury; vascular endothelial cells

Introduction

A growing body of research reveals that ferroptosis is crucial to the pathogenesis of spinal cord injury (SCI) (Chen et al., 2020; Li et al., 2022). Ferroptosis, characterized by iron overload and the accumulation of lipid reactive oxygen species (ROS), is a non-apoptotic form of regulated cell death (Dixon et al., 2012). After SCI, iron overload, overproduction of reactive oxygen species and an imbalance of glutathione peroxidase 4 (GPX4) antioxidant regulation disrupt intracellular redox homeostasis and thus induce ferroptotic cell death (Yao et al., 2019). Recently, studies have revealed that the inhibition of ferroptosis represents novel therapeutic strategies for SCI (Ge et al., 2021). The iron chelator deferoxamine (DFO), lipid peroxidation scavenger SRS-16-86 and free radical scavenger edaravone inhibit ferroptosis in SCI and promote functional recovery (Yao et al., 2019; Zhang et al., 2019; Pang et al., 2022b). However, for specific ferroptotic cell types, previous studies on spinal cord injury have mainly focused on neurons and oligodendrocytes. Both spinal nerve cells and blood vessels are essential for supporting proper spinal cord function, we should also pay attention to whether vascular endothelial cells (ECs) suffer from ferroptosis after SCI. Meanwhile, we should also explore whether ferroptosis inhibitors also mitigate blood-spinal cord barrier (BSCB) disruption in addition to their neuroprotective effects.

The BSCB is a functional structure between blood vessels and nerve tissue of the spinal cord and is composed of vascular ECs, pericytes, astrocyte foot ends, and basement membrane (Bartanusz et al., 2011). Together with neurons, these cells are called the neurovascular unit (NVU). All elements of the NVU contribute to the maintenance of the normal physiological function of the BSCB and protect the neuronal microenvironment (Bartanusz et al., 2011; Younis et al., 2022). Upon BSCB destruction, blood components penetrate the spinal cord, initiating a process of excitatory cytotoxicity, cellular edema, oxidative stress and neuroinflammation, which exacerbates secondary injury in the NVU (Haque et al., 2017; Fan et al., 2022).

ECs are the major component of the BSCB and were shown to undergo ferroptosis-mediated death in the brain (Fang et al., 2022). Brain microvascular endothelial cells (BMVECs) undergo ferroptosis in the oxygen and glucose deprivation hemin-treated model (Chen et al., 2021). In BMVECs isolated from the diabetic mouse brain, the ferroptosis marker Acyl-CoA synthetase long-chain family member 4 (ACSL4) was upregulated, and GPX4, an essential enzyme to remove lipid peroxidation, was downregulated (Abdul et al., 2021). Whether ferroptosis interferes with the NVU and disrupts the BSCB after SCI remains unknown.

[1]Shandong University Center for Orthopedics, Department of Orthopedics, Qilu Hospital of Shandong University, Cheeloo College of Medicine, Shandong University, Jinan, Shandong Province, China; [2]Tianjin Key Laboratory of Spine and Spinal Cord, National Spinal Cord Injury International Cooperation Base, Department of Orthopedics, Tianjin Medical University General Hospital, Tianjin, China
***Correspondence to:** Xue Yao, PhD, yaoxue@sdu.edu.cn; Shiqing Feng, PhD, shiqingfeng@sdu.edu.cn.
https://orcid.org/0000-0003-4904-7697 (Xue Yao); https://orcid.org/0000-0001-9437-7674 (Shiqing Feng)
# These authors contributed equally to this work.

Funding: *This work was supported by the National Natural Science Foundation of China, No. 81972074 (to XY), the Natural Science Foundation of Tianjin, No. 19JCZDJC34900 (to XY), and National Key Research and Development Project of Stem Cell and Transformation Research, No. 2019YFA0112100 (to SF).*
How to cite this article: *Li W, Zhao X, Zhang R, Liu X, Qi Z, Zhang Y, Yang W, Pang Y, Zhao C, Fan B, Ran N, Zhang J, Kong X, Feng S, Yao X (2023) Ferroptosis inhibition protects vascular endothelial cells and maintains integrity of the blood-spinal cord barrier after spinal cord injury. Neural Regen Res 18(11):2474-2481.*

The bEnd.3 cell, a mouse BMVEC line, has basic features of the central nervous system (CNS) microvasculature (Watanabe et al., 2013). Both RSL3 and hemin induced bEnd.3 ferroptosis, with upregulation of 15-lipoxygenase (15-LOX) (Gao et al., 2022). Therefore, here we used bEnd.3 cells to evaluate the effect of liproxstatin-1 (Lip-1) on ECs *in vitro*.

The ferroptosis inhibitor Lip-1 inhibited ferroptosis *in vitro* more potently than other ferroptosis inhibitors, such as DFO, edaravone and ferrostatin-1 (Friedmann Angeli et al., 2014; Jelinek et al., 2018; Fan et al., 2021). Lip-1 promoted neurological recovery and reduced neuroinflammation in subarachnoid hemorrhage (Cao et al., 2021).

In this study, we hypothesized that ferroptosis inhibition by Lip-1 may maintain the integrity of the BSCB and lead to improved functional outcomes after SCI. Our results demonstrated a mechanism of ferroptosis inhibition in exhibiting protective effects as SCI and may provide a new treatment strategy for patients with SCI.

Methods

Animals

Female Wistar rats (8 weeks old, 220–240 g) were acquired from Vital River Laboratory Animal Technology Co., Ltd, China (license No. SYXK (Lu) 20190005). The rats were kept in a controlled environment with a 12-hour/12-hour light-dark cycle. The temperature ranged from 20–25°C, and the humidity ranged from 40–60%. Rats had free access to food and water. All animal procedures were approved by the Animal Ethics Committee of Shandong University Cheeloo College of Medicine on February 27, 2021 (approval No. 21174) and conformed to the National Institutes of Health Guide for the Care and Use of Laboratory Animals (8th ed, National Research Council, 2011). All experiments were designed and reported following the Animal Research: Reporting of *In Vivo* Experiments (ARRIVE) guidelines (Percie du Sert et al., 2020).

SCI model and treatment groups

Anesthesia was administered to rats by 4% inhaled isoflurane (RWD, R510-22, Guangdong, China) until the animals were unconscious, followed by 2% isoflurane during surgery. The dorsal hair was shaved with the T10 vertebrae as the center, and the skin was cut along the midline. The muscle was separated to fully expose the T9–T11 spinous process. The spinal cord was completely exposed by removing the T10 vertebral plate. Rats were fixed at the T9 and T11 spinous processes. A moderate spinal cord contusion was simulated using an NYU Impactor-III (WM Keck, New York, NY, USA) with a 10 g rod at a height of 25 mm by impacting T10. Muscles, fascia and skin were then sutured layer by layer. Bladder were expressed twice daily. Cefuroxime sodium (Servcorp, Nanjing, China) was administered intramuscularly after surgery to prevent infection.

Rats were randomly divided into three groups (n = 36/group): Sham group: rats received only T10 laminectomy without SCI; SCI group: rats received T10 SCI and then an intraperitoneal injection of saline; and Lip-1 group: rats received T10 SCI and then intraperitoneal injection of 10 mg/kg Lip-1. The experimental timeline of the animal experiment is marked in detail in A of each figure. The number of animals for each experiment is indicated in detail in the Figure legend. The ferroptosis inhibitor Lip-1 (C19H21ClN4; Selleck, Houston, TX, USA, Cat# S7699) was dissolved in ethanol and then diluted with saline to 2 mg/mL (10% ethanol as final concentration).

Evans blue test

Rats were anesthetized with 30 mg/kg pentobarbital sodium (6 mg/mL) at 3 days after SCI. BSCB permeability was examined *in vivo* using Evans blue dye (E8010; Solarbio) as previously described (Ye et al., 2016). At 3 days after SCI, the rats were injected with 5 mL/kg of Evans blue dye (10% in saline) via the tail vein. After 3 hours of Evans blue circulation in the body, the rats were anesthetized and transcardially perfused with PBS and 4% paraformaldehyde, and the spinal cord was subsequently removed. The tissues were photographed to visualize dye leakage. Spinal cord tissues were fixed with 4% paraformaldehyde at 4°C for 24 hours and dehydrated through a succession of sucrose concentrations. The tissues were embedded in Sakura Freezing Embedding OCT compound (Sakura, Torrance, CA, USA, Cat# 4583) and coronally sectioned (Leica CM3050S, Wetzlar, Germany) into 10 μm slices. Finally, the amount of Evans blue dye in the spinal cord was observed and quantified at 540 nm under a fluorescence microscope (Olympus OX51, Tokyo, Japan).

Immunofluorescence staining

Rats were anesthetized with 30 mg/kg pentobarbital sodium (6 mg/mL) after SCI. Spinal cord tissues were harvested and embedded in OCT (Sakura, Cat# 4583), followed by sectioning into 10 μm slices (Leica, CM3050S). After fixation in 4% paraformaldehyde for 15 minutes, the samples were blocked and permeabilized (5% goat serum and 0.25% Triton X-100 in TBST) for 1 hour at room temperature. The tissues were incubated with primary antibody (**Table 1**) overnight at 4°C. For immunofluorescence staining of bEnd.3 cells, the cells were washed three times with PBS and fixed with 4% paraformaldehyde for 15 minutes at room temperature. The cells were then blocked and permeabilized (5% goat serum and 0.25% Triton X-100 in TBST) for 1 hour at room temperature. The cells were incubated with primary antibody (**Table 1**) overnight at 4°C. Samples were incubated with the following secondary antibodies for 1 hour at room temperature: Alexa Fluor 555-labeled goat anti-mouse IgG (H+L) (1:500; Abcam, Cambridge, MA, USA, Cat# ab150118, RRID: AB_2714033) and Alexa Fluor 488-labeled goat anti-rabbit IgG (H+L) (1:500; Beyotime Biotechnology, Shanghai, China, Cat# A0423; RRID: AB_2891323). Nuclei were labeled using 4′,6-diamine-2-benzene (DAPI) (Abcam, Cat# ab104139) or Hoechst 33342 (Abcam, Cat# ab228551). Samples were examined using laser confocal microscopy (LSM 980; Carl Zeiss, Oberkochen, Germany). Quantification of $CD68^+$ intensity and MPO^+ intensity was performed at the epicenter and rostral and caudal to the injury site (both 3 mm from the epicenter) of the spinal cord tissue. Quantitative analyses of relative fluorescence intensities were performed using ZEN software (version 3.4, Carl Zeiss).

Table 1 | **Primary antibody information**

Antibody	Host species	Source	Catalog number	RRID	Dilution
Anti-4 HNE	Mouse	Abcam, Cambridge, MA, USA	ab48506	AB_867452	1: 25 (IF)
Anti-MDA	Mouse	Abcam	ab243066	NA	1:200 (IF)
Anti-RECA1	Mouse	Abcam	ab9774	AB_296613	1:200 (IF)
Anti-GPX4	Rabbit	Abcam	ab125066	AB_10973901	1:200 (IF)/ 1:5000 (WB)
Anti-ACSL4	Rabbit	Abcam	ab155282	AB_2714020	1:200 (IF)/ 1:10000 (WB)
Anti-15-LOX	Rabbit	Abcam	ab244205	AB_2910599	1:50 (IF)
Anti-CD68	Rabbit	Abcam	ab125212	AB_10975465	1:500 (IF)
Anti-MPO	Rabbit	Abcam	ab208670	AB_2864724	1:100 (IF)
Anti-NeuN	Mouse	Abcam	ab104224	AB_10711040	1:200 (IF)
Anti-GFAP	Rabbit	Abcam	ab7260	AB_305808	1:200 (IF)
Anti-ZO-1	Rabbit	Proteintech, Rosemont, IL, USA	21773-1-AP	AB_10733242	1:200 (IF)
Anti-beta-actin	Mouse	Proteintech	66009-1-ig	AB_2687938	1:1000 (IF)
Anti-GAPDH	Mouse	Santa Cruz, CA, USA	SC32233	AB_627679	1:500(WB)

4-Hydroxynonenal (4-HNE) and malondialdehyde (MDA) are the lipid peroxidation markers. Rat endothelial cell antigen-1 (RECA-1) is the marker of rat endothelial cells. Glutathione peroxidase 4 (GPX4), acyl-CoA synthetase long-chain family member 4 (ACSL4) and 15-lipoxygenase (15-LOX) are both ferroptosis markers. CD68 is the marker of activated macrophages and microglia. Myeloperoxidase (MPO) is the marker of neutrophil granulocyte. Neuronal nuclear antigen (NeuN) is a marker of neurons and glial fibrillary acidic protein (GFAP) represents astrogliosis. Zonula occludens-1 (ZO-1) is a representative tight junction protein.

Western blotting

Rats were anesthetized with 30 mg/kg pentobarbital sodium (6 mg/mL) 3 days after SCI. Tissues 3 mm from the injury epicenter were obtained and lysed in RIPA Lysis Buffer (Beyotime Biotechnology, Cat# P0013B) containing protease inhibitor (Roche, Basel, Switzerland, Cat# 04693132001). A BCA kit (BL52A, Biosharp, Hefei, Anhui province, China) was used to measure protein concentrations. Sodium dodecyl sulfate polyacrylamide gel electrophoresis (Epizyme Biotech, Shanghai, China, Cat# PG113) was used to separate protein samples denatured in loading buffer (Beyotime Biotechnology, Cat# P0013L). Protein samples were transferred to a polyvinylidene difluoride membrane (Millipore, Billerica, MA, USA, Cat# ISEQ00010). After blocking the membrane in 5% skimmed milk (Beyotime Biotechnology, Cat# P0216) diluted with Tris-buffered saline containing 0.1% Tween-20 at room temperature for 1 hour, the blots were incubated with primary antibodies at 4°C overnight. Antibodies are listed in **Table 1**. Enhanced chemiluminescence (ECL, Millipore, Billerica, MA, USA, Cat# WBKLS0500) was used to view blots. The relative optical densities of proteins of interest were normalized to that of glyceraldehyde-3-phosphate dehydrogenase (GAPDH). Quantification and analysis of proteins was performed using ImageJ (V1.8.0, National Institutes of Health, Bethesda, MD, USA; Schneider et al., 2012).

Detection of glutathione and iron content

Rats were anesthetized with 30 mg/kg pentobarbital sodium (6 mg/mL) at 3 days after SCI. Tissue from the SCI epicenter (50 mg) was collected and homogenized using an automatic TissueLyser (48T, Nanjing Jiancheng Bioengineering Institute, Nanjing, China) for 60 seconds. The glutathione (GSH) and iron contents were detected using the GSH determination kit (Cat# BC1175; Solarbio, Beijing, China) and the iron content kit (Built, Nanjing, Jiangsu Province, China, Cat# A039-2-1), respectively, following the manufacturer's instructions. For *in vitro* samples, bEnd.3 cells were treated with RSL3 only or co-treated with RSL3 and Lip-1 for 24 hours. Approximately 5×10^6 cells were assayed for GSH content (Solarbio, Cat# BC1175) following the manufacturer's instructions.

Cell culture

The bEnd.3 cell line was obtained from the National Collection of

Authenticated Cell Cultures (Shanghai, China, Cat# TCM40, RRID: CVCL_0170). Cells were grown in Dulbecco's modified Eagle's medium (DMEM; BasalMedia, Shanghai, China, Cat# L110KJ) with 10% fetal bovine serum (FBS, Gibco, Grand Island, NY, USA, Cat# F3230) and 1% penicillin-streptomycin (Gibco, Cat# 15140-122) at 37°C and 5% CO_2. In some experiments, bEnd.3 cells were cultured with RSL3 (Selleck, Cat# S8155) and Lip-1 (Selleck, Cat# S7699 for 24 hours in 96-well (5×10^3/well for cell viability detection), 24-well (3×10^4/well for immunofluorescence staining) or 6-well (3×10^5/well for GSH detection) plates.

Cell viability assay

bEnd.3 cells were treated with the ferroptosis inducer RSL3 (100, 50, 25, 12.5, 6.25, 3.125, 1.5625 and 0.78 μM) for 24 hours. The medium was then changed to medium containing 10% Cell Counting Kit-8 reagent (CCK-8, Biosharp, Hefei, Anhui, China, Cat# BS350A). After 1 hour, the optical density (OD) values were measured using a microplate reader (Varioskan LUX, Thermo Fisher Scientific, Waltham, MA, USA). The 50% cytotoxicity concentration (CC50) of RSL3 was calculated by GraphPad Prism 9 (GraphPad Software, San Diego, CA, USA). In other experiments, bEnd.3 cells were co-treated with 7.66 μM RSL3 (CC50) and different concentrations of Lip-1 (0, 0.0001, 0.001, 0.01, 0.1, 1, and 10 μM).

Lipid peroxidation assay

BODIPY 581/591 C11 (Cat# D3861; Invitrogen, Carlsbad, CA, USA) was used to detect lipid peroxidation in bEnd.3 cells. After treatment with drugs, the cells were incubated with 10 μM BODIPY 581/591 C11 at 37°C for 30 minutes. Cells were washed with PBS and observed under a confocal microscope (LSM 980; Carl Zeiss, Oberkochen, Germany). After lipid peroxidation occurred, the fluorescence peak shifts from 590 nm to 510 nm (Drummen et al., 2002).

Hematoxylin and eosin staining

Rats were anesthetized with 30 mg/kg pentobarbital sodium (6 mg/mL) at 8 weeks after SCI. Hematoxylin and eosin staining (Solarbio, Cat# G1120) was used to evaluate the damaged area in the different groups. Spinal cord tissues (both 5 mm from the epicenter to rostral and caudal) were collected from the injury epicenter 8 weeks after SCI. After 24 hours of fixation in 4% paraformaldehyde at 4°C, the tissues were dehydrated through a succession of sucrose concentrations, embedded in Sakura Freezing Embedding OCT compound (Sakura, Torrance, CA, USA, Cat# 4583) and sectioned into 10 μm slices (Leica, CM3050S). Photographs were taken using a microscope (Olympus, VS120, Tokyo, Japan). The cavity area was assessed using ImageJ software.

Basso, Beattie and Bresnahan scoring

Recovery of hindlimb movement was evaluated using Basso, Beattie and Bresnahan (BBB) scoring (Basso et al., 1995). Scoring was conducted on day 1 after SCI and weekly up to 8 weeks. The rats were put on a circular open field, and hindlimb locomotion was observed. Rats were graded by three observers on a BBB grading scale ranging from 0–21, with 0 representing no spontaneous hindlimb movement and 21 representing normal movement. Several aspects of hindlimb movement, including coordination, joint movement, trunk stability, gait pattern and tail control, determined the score.

CatWalk gait analysis

At 8 weeks post-SCI, rats were evaluated using the CatWalk XT system (version 10.6, Noldus, Wageningen, the Netherlands). The CatWalk XT technology includes a platform made of a transparent glass plate that records animal pawprints while walking. High-speed camera on the bottom of the platform records footprints by the intensity of green fluorescence on the glass. A red LED on the ceiling at the top of the glass platform allows for measurement of body contours of the rat. Each rat was trained at least three times before the test. The gait of each rat was recorded with a digital camera and analyzed with CatWalk XT software.

Electrophysiological tests

Nerve conduction function was assessed with electrophysiological tests in rats 8 weeks after SCI. Rats were anesthetized with 30 mg/kg pentobarbital sodium (6 mg/mL). Somatosensory evoked potentials (SEP) and motor evoked potentials (MEP) were determined using an electrophysiological device (YRKJ-G2008; Zhuhai Yiriki Co., Ltd., Guangdong, China) (Yao et al., 2021). For the detection of SEP, stimulating and reference electrodes were placed percutaneously in the gastrocnemius muscle of the lower limb, a grounding electrode was placed subcutaneously in the middle of the back and recording electrodes were placed between the two ears to record peak amplitude and latency. To activate the median nerve in the hind limb, a 0.1-ms-long, 5.1-Hz square wave current was generated using continuous stimulation (2 mA, 50 times). A SEP waveform was received at the recording level. To stimulate the motor areas of the cerebral cortex, a single 5 mA stimulation was applied. The stimulating and reference electrodes were placed subcutaneously between the ears, the grounding electrode was placed subcutaneously in the middle of the back and the recording electrode was placed percutaneously in the gastrocnemius muscle of the lower limb to record the peak amplitude and latency of the MEP.

Statistical analysis

Sample sizes were not predetermined by statistical methods but were consistent with those in a previous publication (Zhao et al., 2022). All behavioral analyses were conducted by investigators blinded to the conditions of the experiments. Statistical analysis was conducted using GraphPad Prism 9 (GraphPad Software, San Diego, CA, USA). One-way analysis of variance followed by Tukey's *post hoc* test was used for comparisons among multiple groups. For behavioral analysis at different times, two-way analysis of variance followed by Tukey's *post hoc* test was used. Data are presented as the mean ± SEM. A *P*-value < 0.05 was considered statistically significant.

Results

Lip-1 reduces BSCB disruption after SCI

Disruption of the BSCB is a major cause of secondary injury in the acute phase of SCI. Thus, ameliorating BSCB injury is a feasible target for SCI repair (Lee et al., 2012; Zhang et al., 2017). We first examined whether Lip-1 influenced BSCB disruption in the acute phase of SCI (**Figure 1A**). We observed leakage of Evans Blue in the SCI group compared with the Sham group, indicating that the barrier function of BSCB was damaged. After Lip-1 treatment, the leakage of Evans Blue had sharply decreased (**Figure 1B**). Evaluation of fluorescence intensity of Evans Blue revealed that the SCI group exhibited significant Evans blue leakage at the epicenter ($P < 0.01$), as well as rostral ($P < 0.01$) and caudal ($P < 0.01$) spinal cord segments; Lip-1 reduced Evans blue leakage at all locations ($P < 0.05$, $P < 0.05$, $P < 0.01$ for epicenter, rostral and caudal areas, respectively; **Figure 1C** and **D**).

Paracellular tight-junction proteins (TJP) such as zonula occludens-1 (ZO-1) are responsible for maintaining the integrity of the BSCB (Zhao et al., 2022). We next examined the effect of Lip-1 on TJP ZO-1 expression in ECs by immunofluorescence staining. ZO-1 expression in ECs was downregulated after injury and this was reversed by Lip-1 administration (Sham *vs*. SCI, $P < 0.001$; SCI *vs*. Lip-1, $P < 0.001$; **Figure 1E** and **F**). Taken together, these results indicate that Lip-1 attenuates BSCB disruption by upregulating ZO-1 expression in ECs.

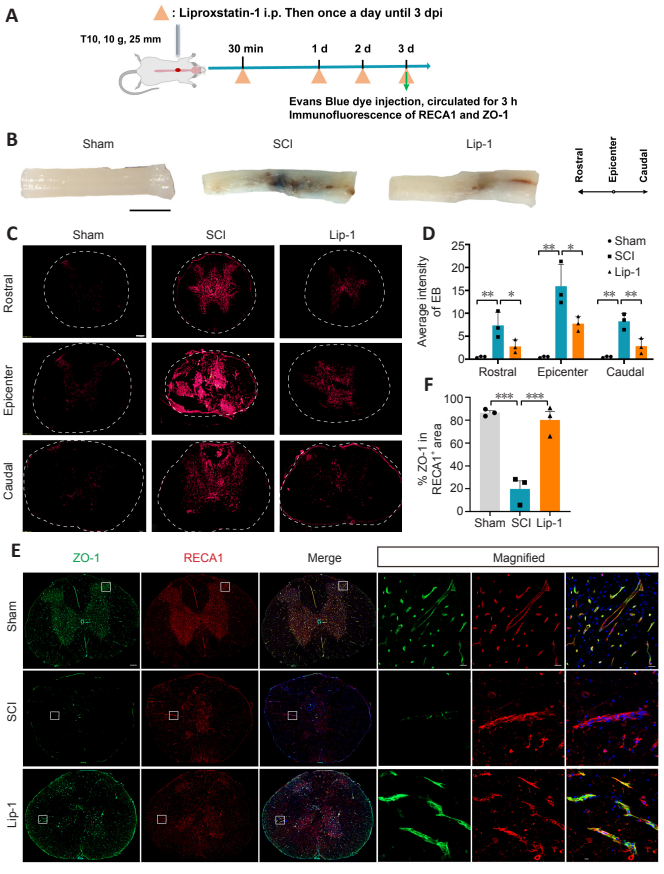

Figure 1 | Liproxstatin-1 reduces blood-spinal cord barrier disruption after SCI.
(A) Experimental design of the analysis of liproxstatin-1 (Lip-1) in blood-spinal cord barrier protection after SCI. Evans blue was injected through the tail vein 3 days after SCI. Spinal cord tissues were removed after 3 hours. (B) The leakage of Evans blue at the lesion site of rats in each group at 3 days post-SCI ($n = 3$). Scale bar:5 mm. (C) Representative fluorescent images of Evans blue leak (red) at the epicenter and rostral and caudal regions. Scale bar: 50 μm. Dotted circles indicate the outline of the transverse section of the spinal cord tissue. (D) Statistical analysis of Evans blue leakage ($n = 3$). (E) Representative immunofluorescence images of zonula occludens-1 (ZO-1; green) and rat endothelium cell antigen-1 (RECA-1; red) staining and cell nuclei (blue) at 3 days after SCI. Scale bars: 200 μm and 20 μm (in magnified figures). Boxes represent the magnified region. (F) Quantitative analysis of the relative fluorescence intensity of ZO-1 in RECA-1$^+$ area ($n = 3$). *$P < 0.05$, **$P < 0.01$, ***$P < 0.001$. Data were analyzed with one-way analysis of variance followed by Tukey's *post hoc* test. SCI: Spinal cord injury.

Lip-1 inhibits the ferroptosis pathway after SCI

Lip-1 is an inhibitor of ferroptosis that reduces lipid peroxidation (Friedmann Angeli et al., 2014). We next examined the effect of Lip-1 on key proteins related to lipid metabolism during the acute phase of SCI (**Figure 2A**). At 3 days post injury, western blot results showed that GPX4 expression was decreased in the SCI group compared to the Sham group ($P < 0.05$), whereas the Lip-1 group showed upregulated GPX4 level compared with the SCI group ($P < 0.05$; **Figure 2B** and **C**). Compared with the sham group, the SCI group showed increased ACSL4 expression ($P < 0.0001$), while compared with the SCI group, the Lip-1 group showed significantly downregulated ACSL4 ($P < 0.01$; **Figure 2D** and **E**). These results demonstrated that Lip-1 inhibited ferroptosis pathway in the acute phase of SCI.

4-Hydroxynonenal (4-HNE) and malondialdehyde (MDA) are metabolic products of lipid peroxidation that damage proteins and nucleic acids in cells and accelerate ferroptosis. Consequently, the 4-HNE and MDA content can reflect the severity of lipid peroxidation. We found that 4-HNE and MDA contents in the spinal cord of rats were significantly lower in the Lip-1 group than those in the SCI group at 3 days after SCI (4-HNE, $P < 0.01$; MDA, $P < 0.001$; **Figure 2F** and **G**, **Additional Figure 1**). We also examined the iron and GSH content in each group 3 days after SCI. GSH concentration was significantly higher in Lip-1-treated SCI rats compared with SCI rats ($P < 0.05$; **Figure 2H**). Additionally, the iron concentration was significantly lower in Lip-1 treated SCI rats compared with SCI rats ($P < 0.01$; **Figure 2I**). These findings showed that Lip-1 reduced ferroptosis after SCI in rats.

Lip-1 inhibits ferroptosis of bEnd.3 cells *in vitro* and increases tight junction protein expression

RSL3 is a GPX4 inhibitor, which leads to ferroptosis onset (Yang et al., 2014). ECs are the major component of the BSCB, and the bEnd.3 cell line is a mouse BMVEC line, which is commonly used to study the CNS microvascular function *in vitro*. To more closely investigate the mechanism by which Lip-1 induces ferroptosis, we induced ferroptosis in bEnd.3 cells using the classic ferroptosis inducer RSL3. We first treated the cells with different concentrations of RSL3; the 50% cytotoxicity concentration (CC50) of RSL3 on bEnd.3 cells was 7.66 μM after 24 hours (**Additional Figure 2A**). We next treated bEnd.3 cells with 7.66 μM RSL3 and different concentrations of Lip-1. The best rescue effect of Lip-1 was 1 μM (**Additional Figure 2B**). Therefore, 7.66 μM of RSL3 and 1 μM of Lip-1 were used for the following experiments.

Immunocytochemistry showed that GPX4 expression in bEnd.3 cells was significantly decreased after RSL3 treatment ($P < 0.01$) and rescued by Lip-1 treatment ($P < 0.05$; **Figure 3A** and **D**). Ferroptosis markers ACSL4 and 15-LOX were elevated in the RSL3-treated group (ACSL4, $P < 0.0001$; 15-LOX, $P < 0.001$), indicating a high level of lipid peroxidation in ferroptotic bEnd.3 cells. After Lip-1 treatment, the two markers were reduced (ACSL4, $P < 0.0001$; 15-LOX, $P < 0.001$; **Figure 3B**, **C**, **E**, **F**). The GSH content was next evaluated; compared with RSL3 treatment alone, Lip-1 significantly increased GSH concentration ($P < 0.0001$; **Figure 3G**). The fluorescent ratio of oxidized BODIPY C11/non-oxidized C11 in RSL3-treated bEnd.3 cells was significantly increased compared with ratios in RSL3 and Lip-1 co-treated bEnd.3 cells ($P < 0.01$; **Figure 3H** and **I**). This indicates a decrease of lipid peroxidation in bEnd.3 cells after Lip-1 treatment. RSL3 significantly decreased expression of the tight junction protein ZO-1, whereas Lip-1 significantly increased the expression of ZO-1 ($P < 0.01$; **Figure 3J** and **K**). Taken together, these results indicate that Lip-1 suppressed RSL3-induced bEnd.3 cell ferroptosis and upregulated the expression of ZO-1.

Ferroptosis inhibition in vascular ECs after SCI

We next examined whether ECs in rats underwent ferroptosis after SCI (**Figure 4A**). We used RECA1 as marker of vascular ECs (Betterton et al., 2022). ACSL4 and 15-LOX were not detected in ECs of the Sham group, whereas their expression increased significantly after SCI (ACSL4, $P < 0.01$; 15-LOX, $P < 0.01$; **Figure 4B–E**). Notably, ECs in the Lip-1 group showed significantly decreased expression of ACSL4 and 15-LOX (ACSL4, $P < 0.05$; 15-LOX, $P < 0.01$; **Figure 4B–E**). These results indicate that in acute SCI, ECs undergo ferroptosis, and Lip-1 inhibition of ferroptosis is associated with decreased expression of ACSL4 and 15-LOX.

Lip-1 inhibits the infiltration of macrophages and neutrophils after SCI

Upon destruction of the BSCB after SCI, blood-derived cells such as macrophages and neutrophils infiltrate into the spinal cord parenchyma to aggravate the inflammatory cascade (Sharma, 2011; Jin et al., 2021). Activated M1 macrophages release a large number of pro-inflammatory factors, and neutrophils infiltrating the spinal cord release MPO, catalyzing an inflammatory response (Beck et al., 2010; Lee et al., 2011; Neirinckx et al., 2014). Therefore, we evaluated the effect of Lip-1 treatment on inflammatory cells by immunofluorescence 3 days after SCI (**Figure 5A**). Many $CD68^+$ macrophages (rostral, $P < 0.001$; epicenter, $P < 0.0001$; caudal, $P < 0.05$; **Figure 5B** and **D**) and MPO+ neutrophils (rostral, $P < 0.001$; epicenter, $P < 0.0001$; caudal, $P < 0.01$; **Figure 5C** and **E**) significantly infiltrated into the spinal cord in the SCI group compared with the Sham group. However, Lip-1 significantly attenuated the increased infiltration of inflammatory cells at the epicenter (CD68, $P < 0.0001$; MPO, $P < 0.0001$), rostral (CD68, $P < 0.001$; $P < 0.01$), and caudal (CD68, $P < 0.05$; MPO, $P < 0.05$). This suggests that Lip-1 attenuates the disruption of the BSCB, thus reducing the infiltration of peripheral-derived inflammatory cells into the spinal cord parenchyma.

Lip-1 alleviates astrogliosis and protects neurons after SCI

Astrocytes are excessively activated following SCI, forming glial scars that hinder axon growth. To evaluate the effect of Lip-1 on astrocytes after SCI, immunofluorescence staining of the astrocyte marker glial fibrillary acidic protein (GFAP) was performed (**Figure 6A**). Eight weeks after SCI, there was obvious astrogliosis around the epicenter; Lip-1 significantly reduced the astrogliosis ($P < 0.05$; **Figure 6B** and **C**). Moveover, Lip-1 reduced the infiltration of peripheral inflammatory cells into the spinal cord parenchyma to improve the inflammatory microenvironment at the injury site, which is a more favorable environment for neuronal survival. Therefore, we further examined the protective effect of Lip-1 on neurons by immunofluorescence staining at 8 weeks after SCI (**Additional Figure 3A**). We found that Lip-1 intervention effectively inhibited the loss of neurons around the lesion ($P < 0.01$; **Additional Figure 3B** and **C**). We conclude that Lip-1 increased neuronal survival and reduced the glia scars after SCI.

Lip-1 spares more spinal cord tissue after SCI

Spinal cord tissue sections from the three groups of rats 8 weeks post-injury were examined by H&E staining. The spinal cord tissue of rats in the Sham group had normal morphology, and no cavity or fissure tissue hyperplasia was seen (**Additional Figure 4**). The spinal cord tissue of rats in the SCI group showed marked structural damage, irregular borders, significant cavity formation and tissue fissure. Notably, the cavity area in the Lip-1 intervention group was approximately 2 times smaller than that in the SCI group ($P < 0.05$).

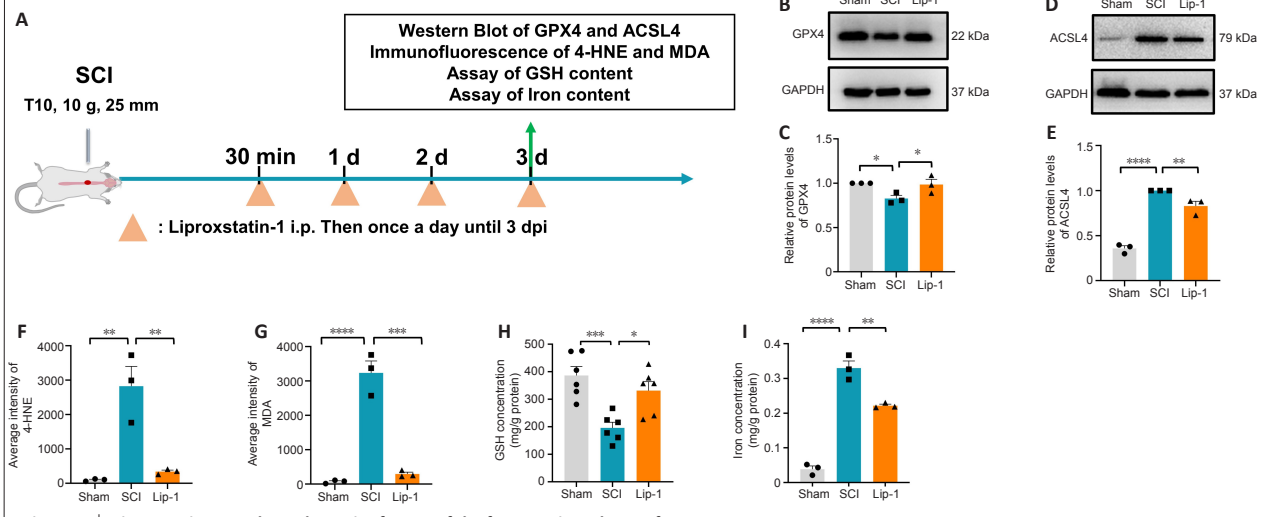

Figure 2 | Liproxstatin-1 regulates the major factors of the ferroptosis pathway after SCI.

(A) Timeline of the ferroptosis pathway analysis in acute SCI in rats. (B, D) Representative western blot image of the expressions of glutathione peroxidase 4 (GPX4) (B) and Acyl-CoA synthetase long-chain family member 4 (ACSL4; D) at 3 days after SCI. (C, E) Quantification of the expression of GPX4 (normalized to the Sham group) and ACSL4 (normalized to the SCI group) in spinal cord tissues in each group ($n = 3$). (F) Quantitative analysis of the fluorescence intensity of 4-hydroxynonenal (4-HNE) in spinal cord tissue ($n = 3$). (G) Quantitative analysis of the fluorescence intensity of malondialdehyde (MDA) in spinal cord tissue ($n = 3$). (H) The concentration of glutathione (GSH) in spinal cord tissue at 3 days after SCI ($n = 6$). (I) The concentration of iron in spinal cord tissue at 3 days after SCI ($n = 3$). *$P < 0.05$, **$P < 0.01$, ***$P < 0.001$, ****$P < 0.0001$. Data were analyzed by one-way analysis of variance followed by Tukey's *post hoc* test. Lip-1: Liproxstatin-1; SCI: spinal cord injury.

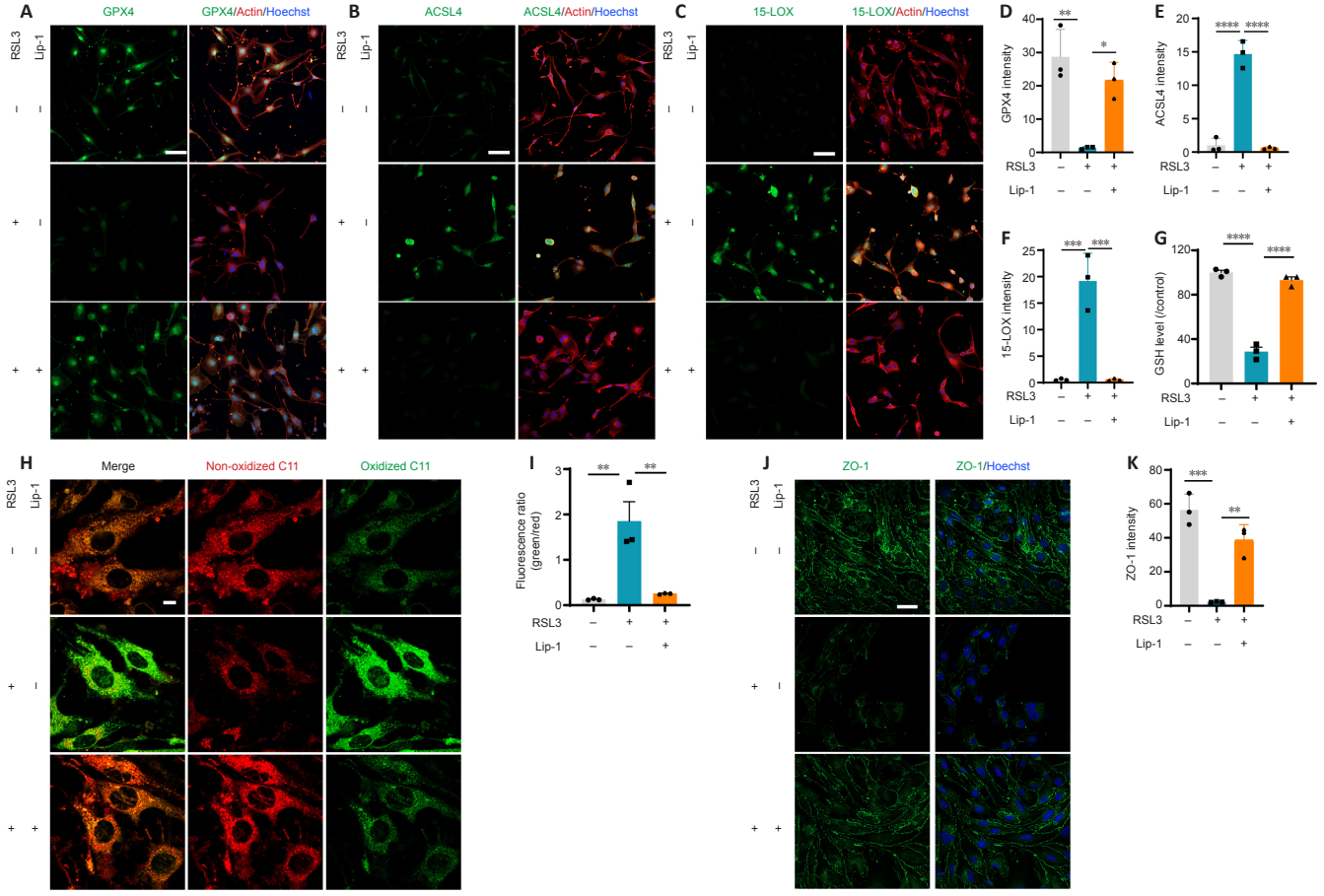

Figure 3 | **Liproxstatin-1 inhibits bEnd.3 cell ferroptosis and increases tight junction protein expression.**
(A–C) Representative immunofluorescence images of glutathione peroxidase 4 (GPX4) (green) (A), Acyl-CoA synthetase long-chain family member 4 (ACSL4; green) (B), 15-lipoxygenase (15-LOX; green) (C), actin (red) and Hoechst (blue) in bEnd.3 cells. Scale bars: 50 μm. (D–F) Quantification of GPX4 (D), ACSL4 (E) and 15-LOX (F) fluorescence intensity in each group (n = 3). (G) The concentration of GSH in each group (n = 3). (H) Representative fluorescence images of BODIPY 581/591 C11 staining. Scale bars: 10 μm. (I) Quantitative analysis of the fluorescence ratio of green (oxidized C11)/red (non-oxidized C11) (n = 3). (J) Representative immunofluorescence images of zonula occludens-1 (ZO-1; green) and Hoechst (blue). Scale bars: 50 μm. (K) Quantification of ZO-1 fluorescence intensity in each group (n = 3). *P < 0.05, **P < 0.01, ***P < 0.001, ****P < 0.0001. Data were analyzed by one-way analysis of variance followed by Tukey's *post hoc* test. Lip-1: Liproxstatin-1.

Lip-1 improves the functional recovery after SCI

To assess whether the ferroptosis inhibitor Lip-1 improves functional recovery after SCI, we used a clinically relevant rat model of contusion SCI. A schematic of the functional analysis is shown in **Figure 7A**. The dose of Lip-1 administrated in SCI (10 mg/kg) was determined from previous applications of Lip-1 in other disease models, such as the Gpx4$^{-/-}$ kidney injury model and the chronic morphine tolerance model (Friedmann Angeli et al., 2014; Chen et al., 2019). Hindlimb locomotion recovery was evaluated using BBB score weekly up to 8 weeks after SCI. While the BBB scores in both the SCI and Lip-1 groups gradually increased over time, the score in the Lip-1 group was markedly higher than that of the SCI group starting from 2 weeks post-injury (**Figure 7B**). Rats in the SCI group had an average BBB score of 8 at 8 weeks post-injury; in rats with Lip-1 treatment, the average BBB score was 12 (P < 0.0001, **Figure 7C**). Approximately 58% of rats in the SCI group had a BBB score less than 9 at 8 weeks post-injury and 42% had a BBB score between 9–13. In the Lip-1 treated group, 67% of rats had a BBB score between 9–13, and 25% had a BBB score above 13 (**Additional Figure 5**). Gait analysis at 8 weeks post-injury showed that rats in the SCI group had uncoordinated gait and extensive hindlimb dragging, while Lip-1-treated rats showed more hindlimb coordination at 8 weeks post-injury (**Figure 7D**). Electrophysiological tests were performed to test the nerve conduction function 8 weeks post-injury (**Figure 7E** and **H**). Compared with the SCI group, the Lip-1 group showed a significantly shortened latency of MEP and SEP (MEP, P < 0.05; SEP, P < 0.0001; **Figure 7F** and **I**). The amplitude of MEP and SEP increased significantly in the Lip-1 group compared with that of the SCI group (MEP, P < 0.01; SEP, P < 0.05; **Figure 7G** and **J**). Taken together, these results indicate that Lip-1 improved hindlimb locomotion and nerve conduction function in rats after SCI.

Discussion

The role of ferroptosis in SCI pathophysiology gains increasing concerns. However, the role of ferroptosis in the BSCB disruption after SCI has been unknown. In this study, we showed that ferroptosis inhibition by Lip-1 maintained BSCB integrity after SCI and reduced vascular endothelial ferroptosis both *in vitro* and *in vivo*. Infiltrated immune cells, both macrophages and neutrophils, were reduced after Lip-1 treatment. Ferroptosis inhibition by Lip-1 led to the functional recovery after SCI.

Our study reveals the novel mechanism of ferroptosis in the BSCB disruption after SCI. The BSCB prevents harmful substances in the blood from entering the spinal cord parenchyma, thereby maintaining a stable environment within the spinal cord (Fan et al., 2018; Montague-Cardoso and Malcangio, 2021). After SCI, damage associated molecular patterns are released to recruit exogenous macrophages, neutrophils and other cells to infiltrate the lesion site to exert an immune response (Zhao et al., 2022). In the process of exerting immune effects, macrophages and neutrophils inevitably produce some inflammatory molecules that are detrimental to the repair of spinal cord tissues. In this study, we found that Lip-1 effectively decreased the number of macrophages and neutrophils in parenchyma to maintain homeostasis of the spinal cord microenvironment, which favors neuronal survival. We speculated that the Lip-1-mediated effect on SCI repair was achieved through protecting the NVU. ACSL4 and 15-LOX are vital enzymes in lipid metabolism-related ferroptosis (Hirschhorn and Stockwell, 2019). We found that Lip-1 treatment downregulated the expression of ACSL4 and 15-LOX in ECs both *in vitro* and *in vivo*. In diabetic mice with disruption of the blood-brain barrier, ACSL4 is upregulated in BMVECs isolated from diabetic mice. DFO treatment lowered the ACSL4 level (Abdul et al., 2021). In the subarachnoid hemorrhage mouse model, 15-LOX is highly expressed in endothelium and reduced by cepharanthine (Gao et al., 2022). ACSL4 synthesizes arachidonic acid and adrenoic acids into arachidonic CoA and adrenoyl CoA, respectively (Doll et al., 2017), which are in turn oxidized by 15-LOX to AA- and AdA-PE-OOH (Kagan et al., 2017). We also found that the expression of GPX4 in ECs was significantly downregulated after RSL3 intervention, while Lip-1 rescued the expression of GPX4, thereby protecting ECs from ferroptosis. GPX4 uniquely catalyzes the reduction of these lipid hydroperoxide levels by converting reduced GSH into GSSG, with the lipid hydroperoxides being converted to either nontoxic alcohols or free hydrogen peroxide (Brigelius-Flohe and Maiorino, 2013). 15-LOX catalyzes AA into two metabolites: 12(S)-hydroxyicosatetraenoic (12(S)-HETE) acid and 15(S)-hydroxyicosatetraenoic acid (15(S)-HETE). A recent study reported overall arachidonic acid metabolism in acute SCI (Pang et al., 2022a). The regulation and function of these AA metabolites in EC ferroptosis need further investigation.

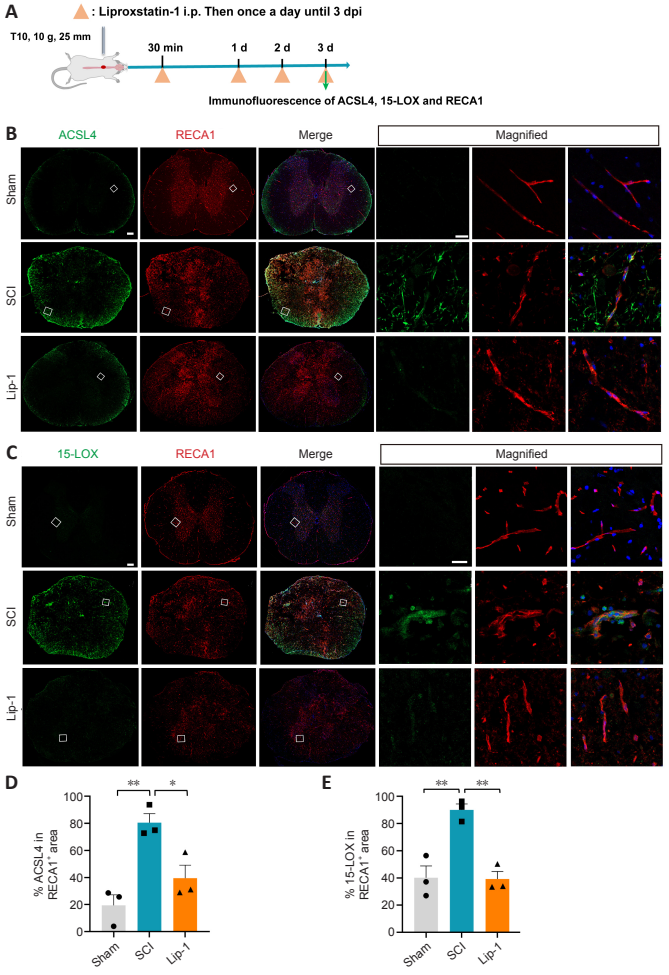

Figure 4 | Liproxstatin-1 regulates ferroptosis of vascular endothelial cells after SCI.
(A) Timeline of the experiments. (B, C) Representative confocal immunofluorescence images of Acyl-CoA synthetase long-chain family member 4 (ACSL4; green) (B), 15-lipoxygenase (15-LOX; green) (C), rat endothelium cell antigen-1 (RECA-1; red) and 4′,6-diamidino-2-phenylindole (DAPI; blue) in the epicenter. Scale bars: 200 μm and 20 μm (in magnified figures). Boxes represent the magnified region. (D, E) Quantitative analysis of the relative fluorescence intensity of ACSL4 (D) and 15-LOX (E) in RECA-1$^+$ area (n = 3). *P < 0.05, **P < 0.01. Data were analyzed by one-way analysis of variance followed by Tukey's *post hoc* test. Lip-1: Liproxstatin-1; SCI: spinal cord injury.

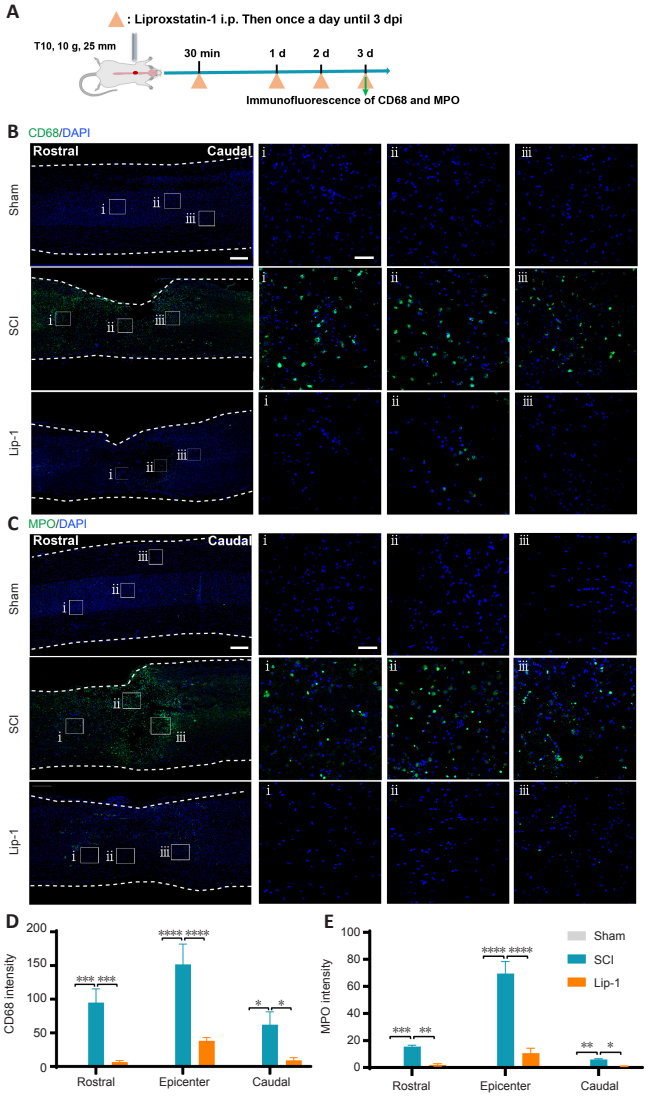

Figure 5 | Liproxstatin-1 inhibits the infiltration of macrophages and neutrophils after SCI.
(A) Timeline of the experiments. (B) Representative confocal immunofluorescence images of CD68 (green) staining and DAPI (blue) in the sagittal view of the spinal cord. Scale bars: 500 μm and 50 μm (i, ii, iii). i, ii, and iii are the magnified images of the region of interest in the leftmost panorama. (C) Representative confocal immunofluorescence images of MPO (green) staining and 4′,6-diamidino-2-phenylindole (DAPI; blue) in the sagittal view of the spinal cord. Scale bars: 500 μm and 50 μm (i, ii, iii). i, ii, and iii are the enlarged images of the region of interest in the leftmost panorama. (D–E) Quantification of CD68$^+$ intensity (D) and MPO$^+$ intensity (E) at the epicenter and rostral and caudal regions (both 3 mm from the epicenter) of the spinal cord tissue (n = 3). *P < 0.05, **P < 0.01, ***P < 0.001, ****P < 0.0001. Data were analyzed by one-way analysis of variance followed by Tukey's *post hoc* test. Lip-1: Liproxstatin-1; MPO: myeloperoxidase; SCI: spinal cord injury.

Neuronal nuclear antigen (NeuN) staining revealed that more neurons survived near the lesion site after treatment with Lip-1 at 8 weeks after SCI. After CNS injury in adult mammals, naive astrocytes are transformed into reactive astrocytes and eventually form scars (Hara et al., 2017). Scar tissue is essential for sealing off injured tissue and restricting damage expansion, but it also impairs axonal regeneration and functional recovery. Our results showed that Lip-1 had a significant effect on reducing the glial scar and promoting the survival of neurons in the tissue adjacent to the injury at 8 weeks post-injury.

This study has some limitations. First, this study focused on the mechanism of Lip-1 regulating EC ferroptosis to rescue BSCB breakdown after SCI. However, we cannot rule out the effect of ferroptosis on other cell types. Inhibition of ferroptosis in neurons and oligodendrocytes promotes the repair of SCI (Ge et al., 2021, 2022). Our previous results showed that Lip-1 inhibited RSL3-induced ferroptosis in the OLN93 cell line (oligodendrocytes) (Fan et al., 2021). Additionally, we previously revealed that DFO prevented erastin-induced ferroptosis of primary neurons (Zhang et al., 2020). Therefore, Lip-1 may be beneficial for multiple cell types besides ECs after SCI. Second, in this study we focus on major ferroptosis regulators such as GPX4, ACSL4 and 15-LOX. We also observed iron overload in the lesioned spinal cord epicenter and this was rescued by Lip-1, so the role of iron metabolism in BSCB and in ECs after SCI is an interesting new direction to explore.NCOA4-mediated ferritinophagy is involved in HUVEC ferroptosis (Qin et al., 2021). Whether ferritinophagy in EC is involved in BSCB disruption is also worthy to study. Third, the NVU involves multiple components and dynamic stages, therefore whether the ferroptosis interferes with astrocyte end-feet, neurovascular remodeling and angiogenesis is not yet clear.

In conclusion, our results expand the role of ferroptosis in SCI by showing that ferroptosis inhibition by Lip-1 maintained the BSCB by inhibiting vascular endothelial ferroptosis. Furthermore, Lip-1 reduced the infiltration

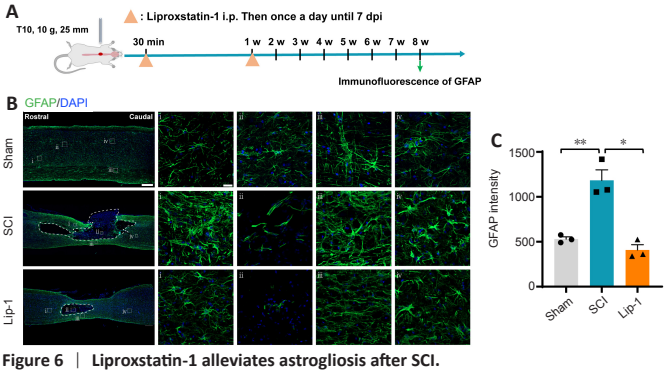

Figure 6 | Liproxstatin-1 alleviates astrogliosis after SCI.
(A) Timeline of the experiments. (B) Representative confocal immunofluorescence images of glial fibrillary acidic protein (GFAP) and cell nuclei at 8 weeks after SCI. Scale bars: 500 μm and 20 μm (i, ii, iii, iv). i, ii, iii and iv are the enlarged images of the region of interest in the leftmost panorama, respectively. (C) Quantification of GFAP-positive intensity at 8 weeks after SCI (n = 3). *P < 0.05, **P < 0.01. Data were analyzed by one-way analysis of variance followed by Tukey's *post hoc* test. Lip-1: Liproxstatin-1; SCI: spinal cord injury; w: week.

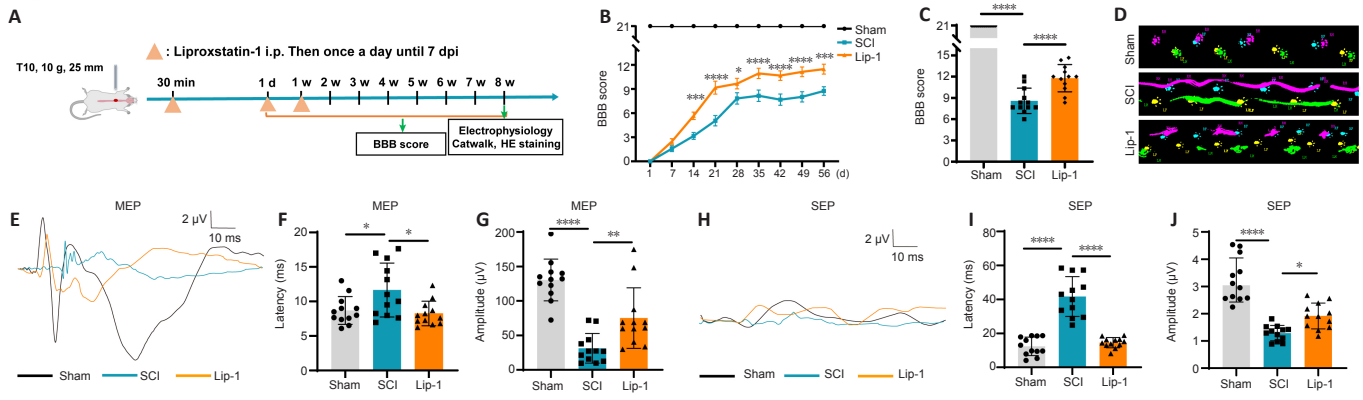

Figure 7 | **Liproxstatin-1 improves functional recovery after SCI.**
(A) Timeline of the functional evaluation after Lip-1 administration in T10 contusive SCI in rats. 7 dpi: 7 days post-injury. (B) Basso, Beattie and Bresnahan (BBB) scores of rats at different time points after injury (n = 12). (C) BBB scores of rats in each group at 8 weeks post-injury (n = 12). (D) Gait analysis of rats in different groups at 8 weeks after injury. Right front paw (blue), right hind paw (purple), left front paw (yellow), left hind paw (green). (E) Representative waveform of motor evoked potentials (MEP) at 8 weeks after injury. (F, G) Quantification of the latency and amplitude of the MEP (n = 12). (H) Representative waveform of somatosensory evoked potentials (SEP) at 8 weeks after injury. (I, J) Quantification of the latency and amplitude of the SEP (n = 12). Two-way analysis of variance followed by Tukey's *post hoc* test for B; one-way analysis of variance followed by Tukey's *post hoc* test for C, F, G, I, and J. *P < 0.05, **P < 0.01, ***P < 0.001, ****P < 0.0001. HE: Hematoxylin and eosin; Lip-1: liproxstatin-1; SCI: spinal cord injury; w: week.

of inflammatory cells, protected neurons, reduced glial scar and promoted functional recovery after SCI. These findings indicate the potential of Lip-1 as a novel and effective treatment for SCI. The clinical translation of Lip-1 in SCI is promising and is generalizable to other neurological diseases that involve ferroptosis.

Author contributions: *XY, SF and XK conceived the project, designed the experiments. WL and XZ analyzed the data and wrote the manuscript with input from all authors. XY and SQF supervised the project and interpreted the results. RZ and YZ performed cellular experiments. WL, XZ and RZ performed the animal experiments. XL and CZ performed animal experiments and behavioral analysis. ZQ, WY and YP reviewed the data and provided critical recommendations for the manuscript. NR, BF and JZ reviewed the data and provided advice. XY and SF provided financial support. All the authors approved the final version of the manuscript.*

Conflicts of interest: *None declared.*

Data availability statement: *All data generated or analyzed during this study are included in this published article and its Additional files.*

Editor's evaluation: *This study demonstrates the potential therapeutic role of Lip-1, as a ferroptosis inhibitor, after spinal cord injury, in preserving spinal cord tissue and improving functional recovery of SCI model rats. The results represent promising implications for the treatment of patients after SCI.*

Additional files:

Additional Figure 1: *Liproxstatin-1 reduces the 4-HNE and MDA content of the rat spinal cord after SCI.*

Additional Figure 2: *Liproxstatin-1 inhibits RSL3 induced bEnd.3 cells ferroptosis.*

Additional Figure 3: *Liproxstatin-1 protects neurons in rats after SCI.*

Additional Figure 4: *Liproxstatin-1 spares more spinal cord tissues in rats after SCI.*

Additional Figure 5: *Liproxstatin-1 improves functional recovery in rats of after SCI.*

References

Abdul Y, Li W, Ward R, Abdelsaid M, Hafez S, Dong G, Jamil S, Wolf V, Johnson MH, Fagan SC, Ergul A (2021) Deferoxamine treatment prevents post-stroke vasoregression and neurovascular unit remodeling leading to improved functional outcomes in type 2 male diabetic rats: role of endothelial ferroptosis. Transl Stroke Res 12:615-630.

Bartanusz V, Jezova D, Alajajian B, Digicaylioglu M (2011) The blood-spinal cord barrier: morphology and clinical implications. Ann Neurol 70:194-206.

Basso DM, Beattie MS, Bresnahan JC (1995) A sensitive and reliable locomotor rating scale for open field testing in rats. J Neurotrauma 12:1-21.

Beck KD, Nguyen HX, Galvan MD, Salazar DL, Woodruff TM, Anderson AJ (2010) Quantitative analysis of cellular inflammation after traumatic spinal cord injury: evidence for a multiphasic inflammatory response in the acute to chronic environment. Brain 133:433-447.

Betterton RD, Abdullahi W, Williams EI, Lochhead JJ, Brzica H, Stanton J, Reddell E, Ogbonnaya C, Davis TP, Ronaldson PT (2022) Regulation of blood-brain barrier transporters by transforming growth factor-beta/activin receptor-like kinase 1 signaling: relevance to the brain disposition of 3-hydroxy-3-methylglutaryl coenzyme a reductase inhibitors (i.e., statins). Drug Metab Dispos 50:942-956.

Brigelius-Flohe R, Maiorino M (2013) Glutathione peroxidases. Biochim Biophys Acta 1830:3289-3303.

Cao Y, Li Y, He C, Yan F, Li JR, Xu HZ, Zhuang JF, Zhou H, Peng YC, Fu XJ, Lu XY, Yao Y, Wei YY, Tong Y, Zhou YF, Wang L (2021) Selective ferroptosis inhibitor liproxstatin-1 attenuates neurological deficits and neuroinflammation after subarachnoid hemorrhage. Neurosci Bull 37:535-549.

Chen B, Wang H, Lv C, Mao C, Cui Y (2021) Long non-coding RNA H19 protects against intracerebral hemorrhage injuries via regulating microRNA-106b-5p/acyl-CoA synthetase long chain family member 4 axis. Bioengineered 12:4004-4015.

Chen X, Zhang B, Liu T, Feng M, Zhang Y, Zhang C, Yao W, Wan L (2019) Liproxstatin-1 attenuates morphine tolerance through inhibiting spinal ferroptosis-like cell death. ACS Chem Neurosci 10:4824-4833.

Chen Y, Liu S, Li J, Li Z, Quan J, Liu X, Tang Y, Liu B (2020) The latest view on the mechanism of ferroptosis and its research progress in spinal cord injury. Oxid Med Cell Longev 2020:6375938.

Dixon SJ, Lemberg KM, Lamprecht MR, Skouta R, Zaitsev EM, Gleason CE, Patel DN, Bauer AJ, Cantley AM, Yang WS, Morrison B 3rd, Stockwell BR (2012) Ferroptosis: an iron-dependent form of nonapoptotic cell death. Cell 149:1060-1072.

Doll S, Proneth B, Tyurina YY, Panzilius E, Kobayashi S, Ingold I, Irmler M, Beckers J, Aichler M, Walch A, Prokisch H, Trümbach D, Mao G, Qu F, Bayir H, Füllekrug J, Scheel CH, Wurst W, Schick JA, Kagan VE, et al. (2017) ACSL4 dictates ferroptosis sensitivity by shaping cellular lipid composition. Nat Chem Biol 13:91-98.

Drummen GP, van Liebergen LC, Op den Kamp JA, Post JA (2002) C11-BODIPY(581/591), an oxidation-sensitive fluorescent lipid peroxidation probe: (micro)spectroscopic characterization and validation of methodology. Free Radic Biol Med 33:473-490.

Fan B, Wei Z, Yao X, Shi G, Cheng X, Zhou X, Zhou H, Ning G, Kong X, Feng S (2018) Microenvironment imbalance of spinal cord injury. Cell Transplant 27:853-866.

Fan B, Wei Z, Feng S (2022) Progression in translational research on spinal cord injury based on microenvironment imbalance. Bone Res 10:35.

Fan BY, Pang YL, Li WX, Zhao CX, Zhang Y, Wang X, Ning GZ, Kong XH, Liu C, Yao X, Feng SQ (2021) Liproxstatin-1 is an effective inhibitor of oligodendrocyte ferroptosis induced by inhibition of glutathione peroxidase 4. Neural Regen Res 16:561-566.

Fang J, Yuan Q, Du Z, Fei M, Zhang Q, Yang L, Wang M, Yang W, Yu J, Wu G, Hu J (2022) Ferroptosis in brain microvascular endothelial cells mediates blood-brain barrier disruption after traumatic brain injury. Biochem Biophys Res Commun 619:34-41.

Friedmann Angeli JP, Schneider M, Proneth B, Tyurina YY, Tyurin VA, Hammond VJ, Herbach N, Aichler M, Walch A, Eggenhofer E, Basavarajappa D, Rådmark O, Kobayashi S, Seibt T, Beck H, Neff F, Esposito I, Wanke R, Förster H, Yefremova O, et al. (2014) Inactivation of the ferroptosis regulator Gpx4 triggers acute renal failure in mice. Nat Cell Biol 16:1180-1191.

Gao S, Zhou L, Lu J, Fang Y, Wu H, Xu W, Pan Y, Wang J, Wang X, Zhang J, Shao A (2022) Cepharanthine attenuates early brain injury after subarachnoid hemorrhage in mice via inhibiting 15-lipoxygenase-1-mediated microglia and endothelial cell ferroptosis. Oxid Med Cell Longev 2022:4295208.

Ge H, Xue X, Xian J, Yuan L, Wang L, Zou Y, Zhong J, Jiang Z, Shi J, Chen T, Su H, Feng H, Hu S (2022) Ferrostatin-1 alleviates white matter injury via decreasing ferroptosis following spinal cord injury. Mol Neurobiol 59:161-176.

Ge MH, Tian H, Mao L, Li DY, Lin JQ, Hu HS, Huang SC, Zhang CJ, Mei XF (2021) Zinc attenuates ferroptosis and promotes functional recovery in contusion spinal cord injury by activating Nrf2/GPX4 defense pathway. CNS Neurosci Ther 27:1023-1040.

Haque A, Capone M, Matzelle D, Cox A, Banik NL (2017) Targeting enolase in reducing secondary damage in acute spinal cord injury in rats. Neurochem Res 42:2777-2787.

Hara M, Kobayakawa K, Ohkawa Y, Kumamaru H, Yokota K, Saito T, Kijima K, Yoshizaki S, Harimaya K, Nakashima Y, Okada S (2017) Interaction of reactive astrocytes with type I collagen induces astrocytic scar formation through the integrin-N-cadherin pathway after spinal cord injury. Nat Med 23:818-828.

Hirschhorn T, Stockwell BR (2019) The development of the concept of ferroptosis. Free Radic Biol Med 133:130-143.

Jelinek A, Heyder L, Daude M, Plessner M, Krippner S, Grosse R, Diederich WE, Culmsee C (2018) Mitochondrial rescue prevents glutathione peroxidase-dependent ferroptosis. Free Radic Biol Med 117:45-57.

Jin LY, Li J, Wang KF, Xia WW, Zhu ZQ, Wang CR, Li XF, Liu HY (2021) Blood-spinal cord barrier in spinal cord injury: a review. J Neurotrauma 38:1203-1224.

Kagan VE, Mao G, Qu F, Angeli JP, Doll S, Croix CS, Dar HH, Liu B, Tyurin VA, Ritov VB, Kapralov AA, Amoscato AA, Jiang J, Anthonymuthu T, Mohammadyani D, Yang Q, Proneth B, Klein-Seetharaman J, Watkins S, Bahar I, et al. (2017) Oxidized arachidonic and adrenic PEs navigate cells to ferroptosis. Nat Chem Biol 13:81-90.

Lee JY, Kim HS, Choi HY, Oh TH, Yune TY (2012) Fluoxetine inhibits matrix metalloprotease activation and prevents disruption of blood-spinal cord barrier after spinal cord injury. Brain 135:2375-2389.

Lee SM, Rosen S, Weinstein P, van Rooijen N, Noble-Haeusslein LJ (2011) Prevention of both neutrophil and monocyte recruitment promotes recovery after spinal cord injury. J Neurotrauma 28:1893-1907.

Li F, Wang H, Chen H, Guo J, Dang X, Ru Y, Wang H (2022) Mechanism of ferroptosis and its role in spinal cord injury. Front Neurol 13:926780.

Montague-Cardoso K, Malcangio M (2021) Changes in blood-spinal cord barrier permeability and neuroimmune interactions in the underlying mechanisms of chronic pain. Pain Rep 6:e879.

National Research Council (2011) Guide for the Care and Use of Laboratory Animals, 8th ed. Washington, DC: The National Academies Press.

Neirinckx V, Coste C, Franzen R, Gothot A, Rogister B, Wislet S (2014) Neutrophil contribution to spinal cord injury and repair. J Neuroinflammation 11:150.

Pang Y, Liu X, Zhao C, Shi X, Zhang J, Zhou T, Xiong H, Gao X, Zhao X, Yang X, Ning G, Zhang X, Feng S, Yao X (2022a) LC-MS/MS-based arachidonic acid metabolomics in acute spinal cord injury reveals the upregulation of 5-LOX and COX-2 products. Free Radic Biol Med 193:363-372.

Pang Y, Liu X, Wang X, Shi X, Ma L, Zhang Y, Zhou T, Zhao C, Zhang X, Fan B, Hao J, Li W, Zhao X, Zhang R, Zhou S, Kong X, Feng S, Yao X (2022b) Edaravone modulates neuronal GPX4/ACSL4/5-LOX to promote recovery after spinal cord injury. Front Cell Dev Biol 10:849854.

Percie du Sert N, Hurst V, Ahluwalia A, Alam S, Avey MT, Baker M, Browne WJ, Clark A, Cuthill IC, Dirnagl U, Emerson M, Garner P, Holgate ST, Howells DW, Karp NA, Lazic SE, Lidster K, MacCallum CJ, Macleod M, Pearl EJ, et al. (2020) The ARRIVE guidelines 2.0: Updated guidelines for reporting animal research. PLoS Biol 18:e3000410.

Qin X, Zhang J, Wang B, Xu G, Yang X, Zou Z, Yu C (2021) Ferritinophagy is involved in the zinc oxide nanoparticles-induced ferroptosis of vascular endothelial cells. Autophagy 17:4266-4285.

Schneider CA, Rasband WS, Eliceiri KW (2012) NIH Image to ImageJ: 25 years of image analysis. Nat Methods 9:671-675.

Sharma HS (2011) Early microvascular reactions and blood-spinal cord barrier disruption are instrumental in pathophysiology of spinal cord injury and repair: novel therapeutic strategies including nanowired drug delivery to enhance neuroprotection. J Neural Transm (Vienna) 118:155-176.

Watanabe T, Dohgu S, Takata F, Nishioku T, Nakashima A, Futagami K, Yamauchi A, Kataoka Y (2013) Paracellular barrier and tight junction protein expression in the immortalized brain endothelial cell lines bEND.3, bEND.5 and mouse brain endothelial cell 4. Biol Pharm Bull 36:492-495.

Yang WS, SriRamaratnam R, Welsch ME, Shimada K, Skouta R, Viswanathan VS, Cheah JH, Clemons PA, Shamji AF, Clish CB, Brown LM, Girotti AW, Cornish VW, Schreiber SL, Stockwell BR (2014) Regulation of ferroptotic cancer cell death by GPX4. Cell 156:317-331.

Yao X, Zhang Y, Hao J, Duan HQ, Zhao CX, Sun C, Li B, Fan BY, Wang X, Li WX, Fu XH, Hu Y, Liu C, Kong XH, Feng SQ (2019) Deferoxamine promotes recovery of traumatic spinal cord injury by inhibiting ferroptosis. Neural Regen Res 14:532-541.

Yao X, Sun C, Fan B, Zhao C, Zhang Y, Duan H, Pang Y, Shen W, Li B, Wang X, Liu C, Zhou H, Kong X, Feng S (2021) Neurotropin exerts neuroprotective effects after spinal cord injury by inhibiting apoptosis and modulating cytokines. J Orthop Translat 26:74-83.

Ye LB, Yu XC, Xia QH, Yang Y, Chen DQ, Wu F, Wei XJ, Zhang X, Zheng BB, Fu XB, Xu HZ, Li XK, Xiao J, Zhang HY (2016) Regulation of caveolin-1 and junction proteins by bFGF contributes to the integrity of blood-spinal cord barrier and functional recovery. Neurotherapeutics 13:844-858.

Younis A, Hardowar L, Barker S, Hulse RP (2022) The consequence of endothelial remodelling on the blood spinal cord barrier and nociception. Curr Res Physiol 5:184-192.

Zhang D, Tang Q, Zheng G, Wang C, Zhou Y, Wu Y, Xuan J, Tian N, Wang X, Wu Y, Xu H, Zhang X (2017) Metformin ameliorates BSCB disruption by inhibiting neutrophil infiltration and MMP-9 expression but not direct TJ proteins expression regulation. J Cell Mol Med 21:3322-3336.

Zhang Y, Sun C, Zhao C, Hao J, Zhang Y, Fan B, Li B, Duan H, Liu C, Kong X, Wu P, Yao X, Feng S (2019) Ferroptosis inhibitor SRS 16-86 attenuates ferroptosis and promotes functional recovery in contusion spinal cord injury. Brain Res 1706:48-57.

Zhang Y, Fan BY, Pang YL, Shen WY, Wang X, Zhao CX, Li WX, Liu C, Kong XH, Ning GZ, Feng SQ, Yao X (2020) Neuroprotective effect of deferoxamine on erastininduced ferroptosis in primary cortical neurons. Neural Regen Res 15:1539-1545.

Zhao C, Zhou T, Zhao X, Pang Y, Li W, Fan B, Li M, Liu X, Ma L, Zhang J, Sun C, Shen W, Kong X, Yao X, Feng S (2022) Delayed administration of nafamostat mesylate inhibits thrombin-mediated blood-spinal cord barrier breakdown during acute spinal cord injury in rats. J Neuroinflammation 19:189.

C-Editor: Zhao M; S-Editor: Li CH; L-Editors: Li CH, Song LP; T-Editor: Jia Y

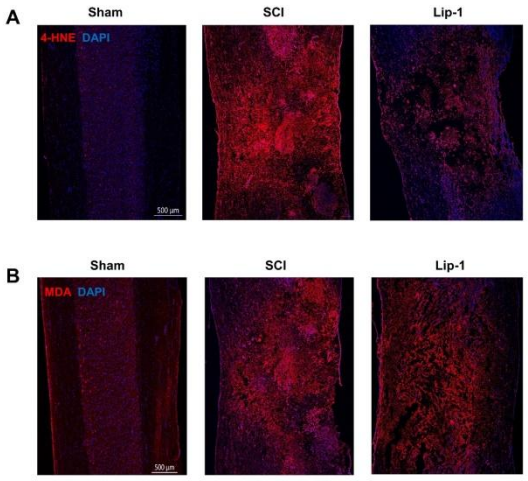

Additional Figure 1 Liproxstatin-1 reduces the 4-HNE and MDA content of the rat spinal cord after SCI.
(A) Representative immunofluorescence image of 4-HNE (red) in spinal cord tissue of each group at 3 days after SCI. (B) Representative immunofluorescence image of MDA (red) in spinal cord tissue of each group at 3 days after SCI. Scale bars: 500 μm. 4-HNE: 4-Hydroxynonenal; DAPI: 4′,6-diamidino-2-phenylindole; Lip-1: liproxstatin-1; MDA: malondialdehyde; SCI: spinal cord injury.

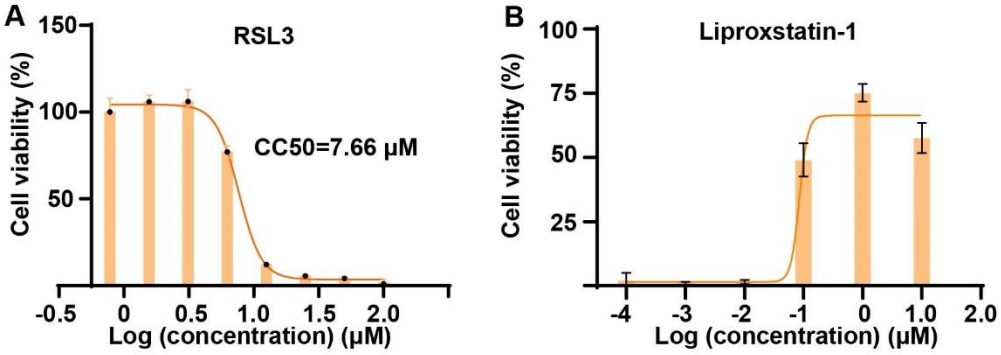

Additional Figure 2 Liproxstatin-1 inhibits RSL3 induced bEnd.3 cells ferroptosis.

(A) Cell viability of bEnd.3 cells treated with different concentrations of RSL3 (50% cytotoxicity concentration [CC50] of RSL3 was 7.66 μM). (B) Cell viability of bEnd.3 cells co-treated with 7.66 μM RSL3 and 0, 0.0001, 0.001, 0.01, 0.1, 1 and 10 μM Lip-1.

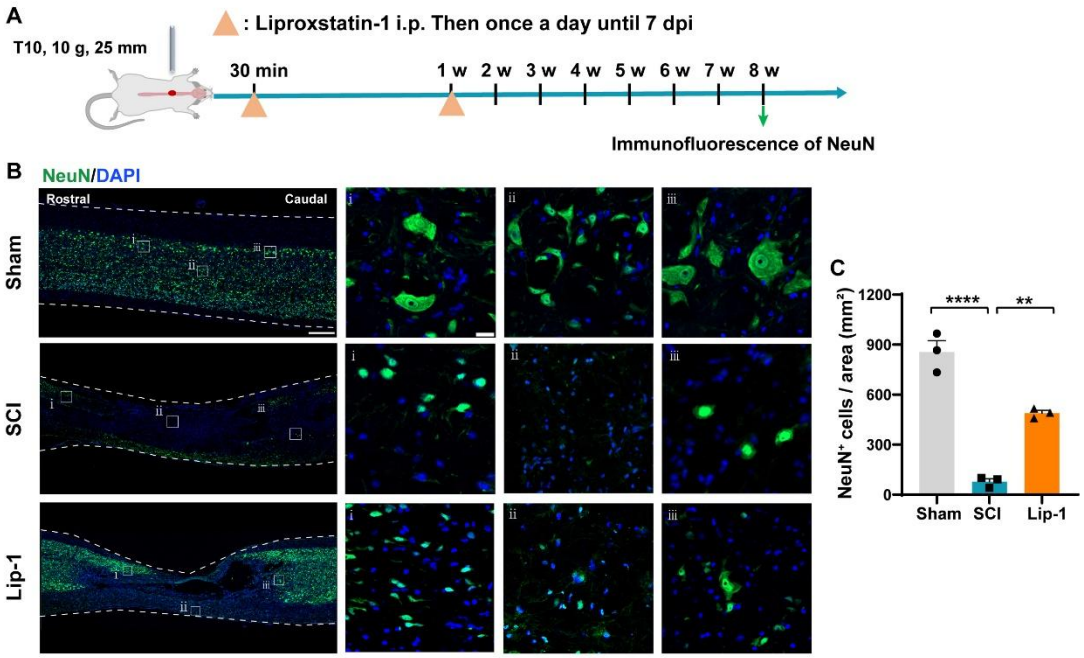

Additional Figure 3 Liproxstatin-1 protects neurons in rats after SCI.

(**A**) Timeline of the experiments. (**B**) Representative confocal immunofluorescence images of NeuN and cell nuclei 8 weeks after SCI. Scale bars: 500 μm and 20 μm (i, ii, iii). i, ii, and iii are the enlarged images of the region of interest in the leftmost panorama, respectively. (**C**) Quantitative analysis of the amount of $NeuN^+$ cells after SCI (n = 3). $^{**}P < 0.01$, $^{****}P < 0.0001$ (one-way analysis of variance followed by Tukey's *post hoc* test). Lip-1: liproxstatin-1; NeuN: Neuronal nuclear antigen; SCI: spinal cord injury.

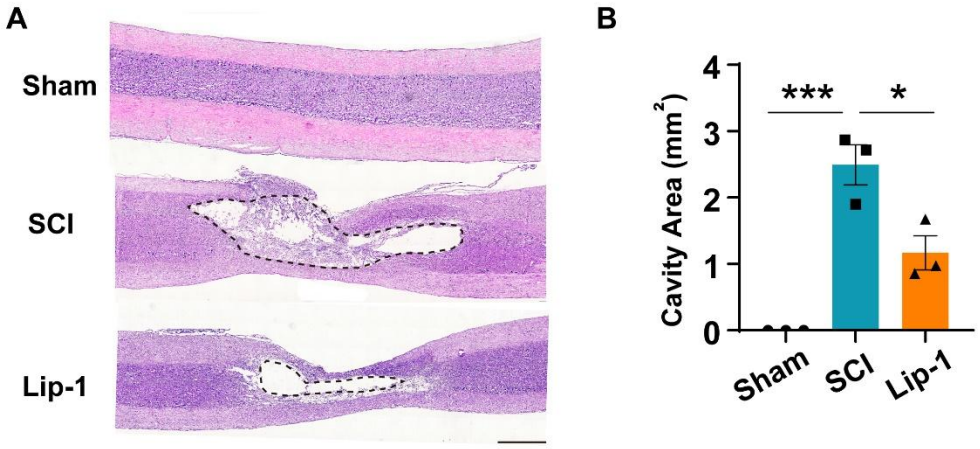

Additional Figure 4 Liproxstatin-1 spares more spinal cord tissues in rats after SCI.

(A) Representative hematoxylin and eosin staining images of rats in each group after 8 weeks post injury. Scale bar: 1 mm. Dotted lines indicate the boundary of the cavity. (B) Quantitative graph of cavity area in each group after 8 weeks post injury (n = 3). *P < 0.05, ***P < 0.001 (one-way analysis of variance followed by Tukey's post hoc test.). Lip-1: Liproxstatin-1; SCI: spinal cord injury.

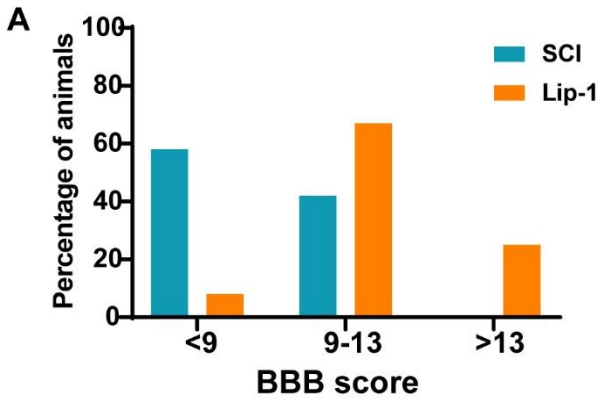

Additional Figure 5 Liproxstatin-1 improves functional recovery in rats of after SCI.

(A) Percentage of animals at successive score segments at 8 weeks after SCI. Lip-1: Liproxstatin-1; SCI: spinal cord injury. BBB: Basso, Beattie and Bresnahan scoring.